Stable, high-power, Yb-fiber-based, picosecond ultraviolet generation at 355 nm using BiB_3O_6

S. Chaitanya Kumar,[1,*] E. Sanchez Bautista,[1] and M. Ebrahim-Zadeh[1,2]

[1]*ICFO—Institut de Ciencies Fotoniques, Mediterranean Technology Park, 08860 Castelldefels, Barcelona, Spain*

[2]*Institucio Catalana de Recerca i Estudis Avancats (ICREA), Passeig Lluis Companys 23, Barcelona 08010, Spain*

**Corresponding author: chaitanya.suddapalli@icfo.es*

Received December 5, 2014; revised December 24, 2014; accepted December 29, 2014;
posted January 6, 2015 (Doc. ID 229161); published January 29, 2015

We report a stable, high-power, high-repetition-rate, picosecond ultraviolet (UV) source at 355 nm based on single-pass sum-frequency generation of a mode-locked Yb-fiber laser at 1064 nm in the nonlinear crystal BiB_3O_6. By performing single-pass second-harmonic generation (SHG) in a 30-mm-long LiB_3O_5 crystal, up to 9.1 W of average green power at 532 nm is obtained at a single-pass SHG efficiency of 54%. The generated green pulses have a duration of 16.2 ps at a repetition rate of 79.5 MHz, with a passive power stability better than 0.5% rms and a pointing stability <12 μrad over 1 h, in high beam quality. The green radiation is then sum-frequency-mixed with the fundamental in a 10-mm-long BiB_3O_6 crystal, providing as much as 1.2 W of average UV power, at an infrared-to-UV conversion efficiency of 7.2%, with a passive power stability better than 0.4% rms over 3 h and a pointing stability <45 μrad over 1 h, in TEM_{00} spatial profile.

OCIS codes: (190.4360) Nonlinear optics, devices; (190.4400) Nonlinear optics, materials; (190.2620) Harmonic generation and mixing.

http://dx.doi.org/10.1364/OL.40.000403

Stable, high-power, picosecond ultraviolet (UV) sources are of great interest for applications ranging from laser micromachining [1] and ultrafast laser patterning [2] to medical diagnostics and pumping of optical parametric oscillators [3]. For many years, the development of such ultrafast sources has relied almost entirely on nonlinear optical techniques based on third (~355 nm) and fourth (~266 nm) harmonic generation of widely established mode-locked Nd/Yb-doped solid-state lasers at ~1064 nm. The rapid advances in fiber laser technology in recent years, however, have paved the way for the replacement of bulky, water-cooled, mode-locked solid-state lasers with compact, air-cooled, ultrafast Yb-fiber lasers at ~1064 nm. With the availability of multiwatt average powers, and the potential for further power scaling, the exploitation of mode-locked Yb-fiber lasers thus offers great promise for the realization of efficient and high-power picosecond UV sources in more practical designs by deploying third and fourth harmonic generation schemes. On the other hand, to fully exploit the advantages of fiber lasers with regard to a compact architecture, simplicity, and portability, it would also be crucial to deploy the most direct nonlinear techniques for UV generation in order to preserve those important merits. To this end, single-pass conversion schemes offer the most effective approach to achieve this goal. We have already verified the viability of such single-pass schemes in combination with continuous-wave (cw) and mode-locked Yb-fiber lasers for efficient generation of high-power cw radiation in the green and UV [4], and high-average-power picosecond pulses in the green [5]. Recently, a fiber-based femtosecond green source was also demonstrated [6].

At the same time, a critical factor in the attainment of the highest nonlinear conversion efficiency and output power is the choice of suitable nonlinear materials. For UV generation, this choice is particularly limited and is especially challenging when low-intensity picosecond pulses at high repetition rates are involved. In addition to a wide transparency in the UV, of paramount importance are a sufficiently high effective nonlinearity, low spatial walk-off, high optical damage threshold, low transmission loss, and high optical quality, as well as chemical and thermal stability. In the absence of suitable periodically poled nonlinear materials offering ready availability, wide transparency, and first-order quasi-phase-matching in the UV, borate-based birefringent crystals have proved the most viable candidates for UV generation. In particular, due to their broad transparency and high damage threshold, β-BaB_2O_4 (BBO) and LiB_3O_5 (LBO) have become materials of choice for the development of high-energy pulsed UV sources, despite their relatively low optical nonlinearities of ~2 pm/V and ~0.7 pm/V, respectively.

On the other hand, the birefringent nonlinear crystal BiB_3O_6 (BIBO), also belonging to the borate family of materials, possesses unique linear and nonlinear optical properties for frequency conversion from the infrared to the visible and UV [4–10]. As a biaxial crystal, it offers highly flexible phase-matching characteristics for various nonlinear interactions in the three optical planes. It has the largest optical nonlinearity of all borate crystals (~3.9 pm/V) [8], with a high bulk UV damage threshold (50 MW/cm^2) [9] and low UV absorption coefficient ($\alpha_{UV} < 0.02$ cm^{-1}) [7], making it a promising candidate for frequency conversion into the UV. Despite a longer UV absorption edge (~280 nm) compared to BBO (~180 nm) and LBO (~160 nm), BIBO can be phase-matched in the optical yz plane under type I ($ee \rightarrow o$) interaction at room temperature using sum-frequency generation (SFG) of infrared and green radiation, to provide UV output at 355 nm with high efficiency. As both input beams at 1064 and 532 nm are *extraordinary*, they experience a spatial walk-off angle of 64.8 mrad and 68 mrad, respectively, corresponding to a small relative walk-off angle of only $\Delta\rho \sim 3.2$ mrad. For SFG to 355 nm, BIBO offers an effective nonlinearity, $d_{eff} \sim 3.2$ pm/V, compared to ~1.8 pm/V in BBO and ~0.7 pm/V in LBO,

with a corresponding figure-of-merit (FOM $= d_{\text{eff}}^2/n^3$) that is 2.5 time larger than BBO and 16.4 times larger than LBO for the same process. This makes BIBO highly attractive for efficient frequency conversion of low-energy, high-repetition-rate, picosecond pulses into the UV [10]. Recently, two new borate-based nonlinear crystals, CsB_3O_5 (CBO) and $La_2CaB_{10}O_{19}$ (LCB), were reported to generate watt-level picosecond UV radiation at 355 nm [11,12]. Although their UV absorption edge extends down to ~170 nm, these materials are as yet not commercially available. Moreover, the effective nonlinearities, $d_{\text{eff}} \sim$ 1.1 pm/V and ~1.05 pm/V for CBO and LCB, respectively, are both ~3 times lower than BIBO. For SFG to 355 nm, the *FOM* of LCB is 9.5 times lower than BIBO. Moreover, LCB is reported to exhibit 3 times higher two-photon absorption coefficient in the UV compared to BIBO, which could seriously affect power stability [13], and thus also the potential for power scaling, while CBO is hygroscopic [11]. As such, it is imperative to investigate the viability of alternative nonlinear materials with ready availability, such as BIBO, for the generation of high-average-power, high-repetition-rate, picosecond UV pulses at 355 nm.

Here, we report such a source using BIBO as the nonlinear crystal pumped by a mode-locked Yb-fiber laser at 1064 nm. The compact and stable UV source is based on a practical and simplified architecture using single-pass second harmonic generation (SHG) in LBO followed by SFG in BIBO, providing as much as 1.2 W of average UV power at 355 nm at an infrared-to-UV conversion efficiency of 7.2%. The generated UV exhibits a passive power stability better than 0.4% rms over 3 h and a pointing stability <45 μrad over 1 h in TEM_{00} spatial profile. To the best of our knowledge, this is the first attempt to generate high-average-power UV radiation in BIBO below 370 nm [14].

The schematic of the experimental setup is shown in Fig. 1. The fundamental source is a mode-locked Yb-fiber laser delivering up to 20 W of average power at 1064 nm in pulses of 20 ps duration at 79.5 MHz repetition rate. The laser has a double-peaked spectrum with a full width at half-maximum (FWHM) bandwidth of ~1.4 nm. The output power is adjusted using a combination of a half-wave plate and a polarizing beam-splitter cube. A second half-wave plate is used to obtain the required polarization for phase-matching in the nonlinear crystals. The LBO crystal for SHG is 30-mm-long with an aperture of 3 mm × 4 mm. It is cut at $\theta = 90°(\varphi = 0°)$ for type I ($oo \rightarrow e$) noncritical phase-matching (NCPM) in the optical xy plane at 148.2°C. In this interaction, the fundamental is polarized as an *ordinary* wave, while the second harmonic beam is *extraordinary*.

The SFG stage comprises a 10-mm-long, 3-mm-wide, and 3-mm-thick BIBO crystal, cut at $\theta = 146.3°(\varphi = 90°)$ in the optical yz plane for type I ($ee \rightarrow o$) sum-frequency mixing of 1064 and 532 nm to generate UV output at 354.7 nm. In this interaction, both fundamental and second harmonic are *extraordinary*, while the SFG output is *ordinary*. In order to achieve identical polarizations at fundamental as well as second harmonic beam for phase-matching in the SFG stage, we used a pair of dual-wavelength wave-plates (DWPs), which simultaneously provide quarter-wave rotation at 532 nm and half-wave rotation at 1064 nm, as shown in the inset of Fig. 1. Unlike the LBO crystal in the SHG stage, with NCPM at high temperature, the BIBO crystal in the SFG stage is phase-matched by angular interrogation at room temperature. The end-faces of both crystals are antireflection (AR)-coated ($R < 0.1\%$) at 1064 and 532 nm, while the BIBO faces are also AR-coated at 354.7 nm. The fundamental beam is focused at the center of the LBO crystal to a waist radius of $w_{o1} \sim 34$ μm, corresponding to a focusing parameter of $\xi \sim 2.74$ [15], to provide SHG output at 532 nm. The generated second harmonic beam and the undepleted fundamental are then refocused into the BIBO crystal in the SFG stage. For this purpose, two plano-concave mirrors, M_1 and M_2, are used to provide an elliptic beam waist inside the BIBO crystal. Both mirrors are coated for high reflectivity ($R > 99\%$) at 1064 and 532 nm and mounted on translation stages, so as to adjust the intercrystal spacing between the SHG and SFG stage. The radius of curvature of M_1 and M_2 are $r = 150$ mm and 200 mm, respectively. The generated UV radiation is then separated from the fundamental and second harmonic beams using dichroic mirrors, M_T ($R > 99\%$ at 355 nm, $T > 99\%$ at 1064 and 532 nm), and further filtered using FGUV11 glass, F, while mirrors, M_S ($R > 99\%$ at 532 nm, $T > 99\%$ at 1064 nm), separate the SH wavelength from the fundamental.

In order to characterize the generated UV output, we first investigated the performance of the SHG stage. The power scaling and efficiency results for single-pass SHG in LBO are shown in Fig. 2. The green power increases quadratically, as expected, providing a maximum of 9.1 W for the highest fundamental power of 16.8 W at the input to the LBO crystal, at a single-pass conversion efficiency of 54%. Also shown in Fig. 2 is the variation of

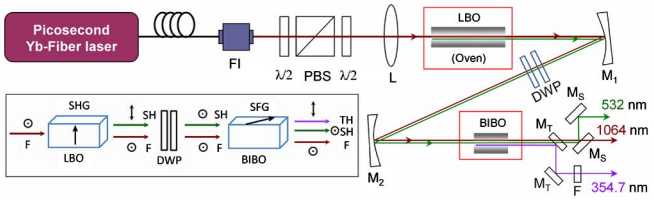

Fig. 1. Configuration of picosecond UV source based on single-pass SHG/SFG in LBO/BIBO. FI, Faraday isolator; $\lambda/2$, half-wave plates; PBS, polarizing beam splitter; L, lens; DWP, dual-wavelength wave-plates; $M_{1,2}$, plano–concave mirrors; M_S, green separation mirrors; M_T, UV separation mirrors; F, UV filter.

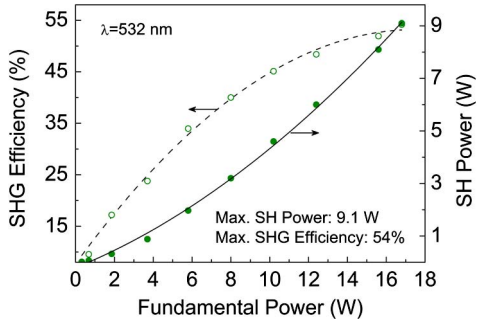

Fig. 2. Variation of the second harmonic power and SHG efficiency as a function of fundamental power.

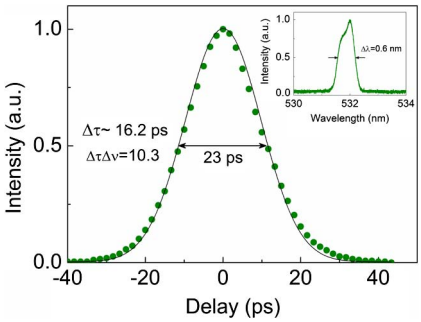

Fig. 3. Typical autocorrelation trace of the second harmonic at 532 nm with a duration of 16.2 ps (×1.414, assuming a Gaussian pulse shape). Inset: second harmonic spectrum measured at a central wavelength of 532 nm with a FWHM bandwidth of 0.6 nm.

SHG efficiency with fundamental power, which is expected to be linear. However, at high input power levels the variation is no longer linear, implying saturation, as also observed previously [5,9,12]. We performed temporal and spectral characterization of the generated green beam. Figure 3 shows a typical autocorrelation profile at 532 nm, indicating a FWHM duration of 23 ps. Assuming a Gaussian pulse shape, this corresponds to a pulse duration of 16.2 ps. This value was also confirmed by repeating the measurement at different fundamental power levels. The second harmonic spectrum, measured using a visible spectrum analyzer, is centered at 532 nm with a FWHM bandwidth of 0.6 nm, as shown in the inset of Fig. 3, resulting in $\Delta\nu\Delta\tau \approx 10.3$. The large time-bandwidth product is essentially attributed to the non-transform-limited ($\Delta\nu\Delta\tau \approx 7.4$) fundamental pulses from the Yb-fiber laser.

We also recorded the long-term power stability of the generated green beam at 9 W of average power, with the result shown in Fig. 4. As can be seen, the output power at 532 nm exhibits excellent passive stability of better than 0.5% rms over 16 h, compared to 0.24% rms for the fundamental measured over the same period of time. The far-field energy distribution of the generated green beam, measured at 9 W and at ~1 m from the LBO crystal, is shown in inset (a) of Fig. 4, confirming a TEM_{00} profile with a circularity of >97% owing to NCPM in LBO. Also shown in inset (b) of Fig. 4 is the green beam pointing stability. Using an $f = 125$ mm focal length lens and a scanning beam profiler, we measured the deviation in the green beam centroid position, resulting in a pointing stability <12 μrad in the x direction and <10 μrad in the y direction.

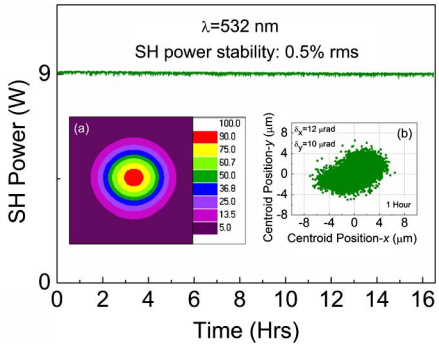

Fig. 4. Long-term power stability of the green source over 16 h. Insets: (a) SH beam profile, and (b) pointing stability measured over 1 h.

After the complete characterization of the SHG output, we performed optimization of the SFG stage. In order to maximize SFG efficiency, ideally one green photon would be required for every fundamental photon to realize sum-frequency mixing, thereby generating one UV photon. This implies an optimum 1064/532 nm power ratio of 1/2. In the SHG stage, we generated 9.1 W of green power, with 7.6 W of unconverted fundamental remaining for SFG, resulting in a power ratio of ~1/1.2. Further, the maximum efficiency for SFG is achieved when the interacting beams have optimum overlap throughout the length of the crystal, but spatial walk-off significantly reduces this overlap. As both beams (1064 and 532 nm) at the input to the BIBO crystal are *extraordinary*, they experience a small relative walk-off angle, $\Delta\rho \sim 3.2$ mrad. This results in an offset of 650 and 680 μm at the exit face of the 10-mm-long BIBO crystal for the fundamental and second harmonic beams, respectively. As such, larger beam diameters are required to offset spatial walk-off, which in turn leads to reduced efficiency due to lower intensities. Hence, we used the mirrors, M_1 and M_2, at small angles to focus the undepleted fundamental as well as the second harmonic beam to an elliptic waist, resulting in a horizontal focused radius of $w_{o2} \sim 63 \times 187$ μm. The UV power scaling results as a function of the fundamental power, under this focusing configuration, are shown in Fig. 5, where the data have been corrected for the transmission loss of the UV filter, F. As is evident, the UV average power increases with the fundamental, reaching a maximum of 1.2 W for the highest input Yb-fiber power of 16.8 W, at an infrared-to-UV single-pass conversion efficiency of 7.2%. This efficiency is comparable to that obtained in Ref. [12] at similar average input power, with a corresponding peak pulse power of 18.7 kW in a 17.6-mm-long LCB crystal. This is ~1.8 times larger than the input peak power of 10.5 kW used here in a 10-mm-long BIBO crystal. The UV spectrum centered at 355 nm, measured using a UV–visible spectrometer, is shown in the inset of Fig. 5, indicating a bandwidth of ~1 nm (FWHM), limited by the instrument resolution.

Further, we recorded the passive long-term power stability of the generated UV output over 14 h. As can be seen in Fig. 6, the UV power exhibits a long-term drift resulting in a slow decline from 1.2 W down to ~1 W after

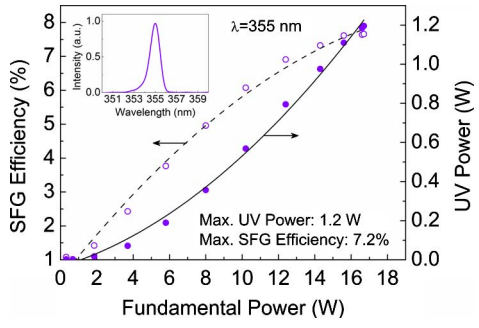

Fig. 5. Variation of the UV power and efficiency as a function of fundamental power. Inset: UV spectrum centered at 355 nm.

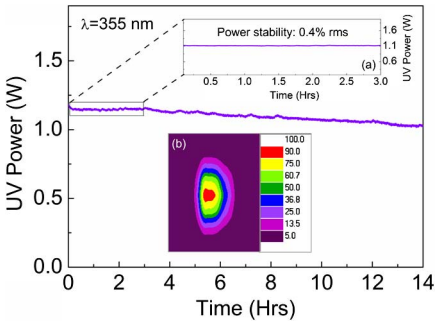

Fig. 6. Long-term power stability of the UV source over 14 h. Insets: (a) UV power stability over 3 h, (b) TH beam profile measured using a scanning beam profiler.

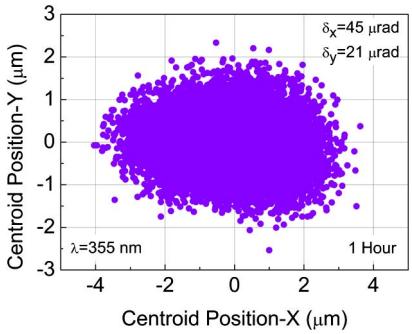

Fig. 7. Beam pointing stability of the UV output beam generated by BIBO in the SFG stage measured over 1 h.

14 h. By translating the crystal to focus the input beams to a new position inside the BIBO, we could readily recover the maximum UV power. This long-term drift in UV power could be attributed to photo-induced damage [16], two-photon absorption, or dynamic color center formation, previously observed in borate crystals [17]. However, photo-induced damage in BIBO can be repaired with high-temperature annealing at ~300°C [16], thus potentially improving the long-term power stability. Confirmation of the origin of the long-term power drop requires further studies. Nevertheless, during the first 3 h of the measurement, the UV power is recorded to exhibit passive power stability better than 0.4% rms, as shown in inset (a) of Fig. 6. To the best of our knowledge, such power stability measurements as performed here have not been previously reported for UV generation in earlier works involving any other nonlinear material at any power level. We have not observed any permanent damage in the BIBO crystal even after >14 h of continuous operation and repeated operation over many days and weeks. Also shown in the inset (b) of Fig. 6 is the UV beam profile measured 50 cm from the BIBO crystal, at >1 W of UV power, using a scanning beam profiler. The UV beam is recoded to exhibit a circularity of ~47% owing to the spatial walk-off in BIBO, but this can be readily circularized using suitable cylindrical optics. Finally, we measured the beam pointing stability of the generated UV output. We recorded the deviation in the centroid position by focusing the UV beam with a $f = 50$ mm focal length lens and using a scanning beam profiler, resulting in a pointing stability <45 μrad in the x direction and <21 μrad in the y direction, as shown in Fig. 7.

In conclusion, we have demonstrated a compact, stable, high-power picosecond UV source at 355 nm based on single-pass SFG in BIBO pumped by a mode-locked Yb-fiber laser at 1064 nm. The combination of Yb-fiber laser with single-pass conversion results in a highly simplified and practical design, preserving the key advantages of fiber technology with regard to a compact, portable, and air-cooled architecture. We have generated up to 1.2 W of UV average power at 79.5 MHz at an infrared-to-UV conversion efficiency of 7.2%, with power stability better than 0.4% rms over 3 h and pointing stability better than 45 μrad over 1 h, in TEM_{00} spatial profile. The generated UV power could be further enhanced by using a delay line to improve temporal overlap of 1064 and 532 nm pulses in the crystal, as well as deploying a two-crystal compensation scheme to further minimize the residual spatial walk-off in BIBO. With the power scaling potential of Yb-fiber lasers, further increase in the UV power to multiwatt levels is also a clear possibility without damage to the BIBO crystal. The obtained results confirm the viability of BIBO as a highly attractive material for efficient generation of low-intensity picosecond pulses in the UV.

We acknowledge support from the Ministry of Economy and Competitiveness (MINECO), Spain, through project OPTEX (TEC2012-37853).

References

1. T. Rauch and R. Delmdahl, Laser Tech. J. **6**, 20 (2009).
2. D. Karnakis, A. Kearsley, and M. Knowles, J. Laser Micro/Nano Eng. **4**, 218 (2009).
3. V. Kubecek, S. Kumazaki, A. Agnesi, G. C. Reali, Y. Takagi, and K. Yoshihara, J. Opt. Soc. Am. B **10**, 2211 (1993).
4. S. Chaitanya Kumar, K. Devi, and M. Ebrahim-Zadeh, Opt. Lett. **38**, 5114 (2013).
5. S. Chaitanya Kumar and M. Ebrahim-Zadeh, Laser Phys. **24**, 025401 (2014).
6. A. N. Chaitanya, A. Aadhi, R. P. Singh, and G. K. Samanta, Opt. Lett. **39**, 5419 (2014).
7. M. Ghotbi, Z. Sun, A. Majchrowski, E. Michalski, I. V. Kityk, and M. Ebrahim-Zadeh, Appl. Phys. Lett. **89**, 173124 (2006).
8. V. Petrov, M. Ghotbi, O. Kokabee, A. Esteban-Martin, F. Noack, A. Gaydardzhiev, I. Nikolov, P. Tzankov, I. Buchvarov, K. Miyata, A. Majchrowski, I. Kityk, F. Rotermund, E. Michalski, and M. Ebrahim-Zadeh, Laser Photon. Rev. **4**, 53 (2010).
9. M. Peltz, J. Bartschke, A. Borsutzky, R. Wallenstein, S. Vernay, T. Salva, and D. Rytz, Appl. Phys. B **81**, 487 (2005).
10. G. K. Samanta, S. Chaitanya Kumar, A. Aadhi, and M. Ebrahim-Zadeh, Opt. Express **22**, 11476 (2014).
11. L. Guo, G. L. Wang, H. B. Zhang, D. F. Cui, Y. C. Wu, L. Lu, J. Y. Zhang, J. Y. Huang, and Z. Y. Xu, Appl. Phys. B **88**, 197 (2007).
12. K. Li, L. Zhang, D. Xu, G. Zhang, H. Yu, Y. Wang, F. Shan, L. Wang, C. Yan, Y. Wu, X. Lin, and J. Yao, Opt. Lett. **39**, 3305 (2014).
13. I. V. Kityk, A. Majchrowski, E. Michalski, D. Kasprowicz, M. Drozdowski, J. Kisielewski, T. Lukasiewicz, and B. Sahraoui, J. Phys. Chem. B **110**, 9090 (2006).
14. M. Ghotbi and M. Ebrahim-Zadeh, Opt. Lett. **30**, 3395 (2005).
15. G. D. Boyd and D. A. Kleinman, J. Appl. Phys. **39**, 3597 (1968).
16. J. H. Jang, I. H. Yoon, and C. S. Yoon, Opt. Mater. **31**, 781 (2009).
17. M. Takahashi, A. Osada, A. Dergachev, P. F. Moulton, M. Cadatal-Raduban, T. Shimizu, and N. Sarukura, J. Cryst. Growth **318**, 606 (2011).